This is a self-archived version of an original article. This version may differ from the original in pagination and typographic details.

Author(s): Cerone, Giacinto Luigi; Giangrande, Alessandra; Vieira, Taian; Pisaturo, Domenico; Ionescu, Mihai; Gazzoni, Marco; Botter, Alberto

Title: Design of a programmable and modular neuromuscular electrical stimulator integrated into a wireless Body Sensor Network

Year: 2021

Version: Published version

Copyright: © 2021 the Authors

Rights: CC BY-NC-ND 4.0

Rights url: https://creativecommons.org/licenses/by-nc-nd/4.0/

Please cite the original version:

Cerone, G. L., Giangrande, A., Vieira, T., Pisaturo, D., Ionescu, M., Gazzoni, M., & Botter, A. (2021). Design of a programmable and modular neuromuscular electrical stimulator integrated into a wireless Body Sensor Network. IEEE Access, 9, 163284-163296. https://doi.org/10.1109/access.2021.3133096

IEEE *Access*
Multidisciplinary : Rapid Review : Open Access Journal

Design of a programmable and modular neuromuscular electrical stimulator integrated into a wireless Body Sensor Network

Giacinto Luigi Cerone[1], Member, IEEE, Alessandra Giangrande[1-2], Taian Vieira[1], Domenico Pisaturo[3], Mihai Ionescu[3], Marco Gazzoni[1], Member, IEEE, and Alberto Botter[1], Member, IEEE

[1] LISiN – Laboratory for Engineering of the Neuromuscular System, Department of Electronica and Telecommunications, Politecnico di Torino, 10129, Turin, Italy

[2] University of Jyväskylä, Faculty of Sports and Health Science, FI-40014, Jyväskylä, Finland

[3] CIONIC Inc. 94133, San Francisco, California, USA

Corresponding author: G.L. Cerone (e-mail: giacintoluigi.cerone@polito.it).

ABSTRACT Neuromuscular electrical stimulation finds application in several fields, from basic neurophysiology, to motor rehabilitation and cardiovascular conditioning. Despite the progressively increasing interest in this technique, its State-of-the-Art technology is mainly based on monolithic, mostly wired devices, leading to two main issues. First, these devices are often bulky, limiting their usability in applied contexts. Second, the possibility of interfacing these stimulation devices with external systems for the acquisition of electrophysiological and biomechanical variables to control the stimulation output is often limited. The aim of this work is to describe the design and development of an innovative electrical stimulator, specifically developed to contend with these issues. The developed device is composed of wireless modules that can be programmed and easily interfaced with third-party instrumentation. Moreover, benefiting from the system modular architecture, stimulation may be delivered concurrently to different sites while greatly reducing cable encumbrance. The main design choices and experimental tests are documented, evidencing the practical potential of the device in use-case scenarios.

INDEX TERMS Electrical Stimulation, Functional Electrical Stimulation, Medical Instrumentation for electrical stimulation, Modular wireless systems, Neuromuscular System, Rehabilitation

I. INTRODUCTION

Neuromuscular electrical stimulation has found noteworthy applications, from basic physiology to motor rehabilitation and cardiovascular conditioning [1]–[5]. Given this broad spectrum of applications involving both external [6], [7] and implantable systems [8]–[10], defining a single, optimal stimulation device is unlikely viable, as it would need to conform to different, specific needs. While, for example, the counting of motor units using incremental stimulation demands fine increases in the current intensity of a single, stimulation channel [5], [11], in functional electrical stimulation (FES) protocols issuing high-current pulses to several skeletal muscles are often required [12], [13]. Specifically concerning FES treatments [14], stimulation devices should ideally: i) provide the possibility of controlling stimulation output according to either a biomechanical or electrophysiological variable, necessary for closed-loop protocols [15], [16]; ii) convey several stimulation channels

allowing to activate the main muscle groups involved in the movement of interest [4]. Currently available stimulators do not seem to meet the requirements for general use. More specifically, to assuage the demands of different application scenarios, these devices should feature three technical aspects: i) high quality of the stimulation pulse required for basic neurophysiological study (e.g. DS7R, Digitimer Ltd, Hertfordshire, UK); ii) multi-channel programmable stimulation needed for FES applications (e.g. RehaStim, Hasomed GmbH, Magdeburg, Germany), and iii) intuitive integration and compatibility with third-party devices used to measure bio-signals and trigger the stimulation onset (e.g. RehaMove, Hasomed GmbH, Magdeburg, Germany). Although the development and use of programable stimulators have been reported in the literature [6], [7], [17]–[20], these devices do not include the possibility to integrate third-party sensing units and therefore do not allow for the control of stimulation patterns from biomechanical signals, such as joint
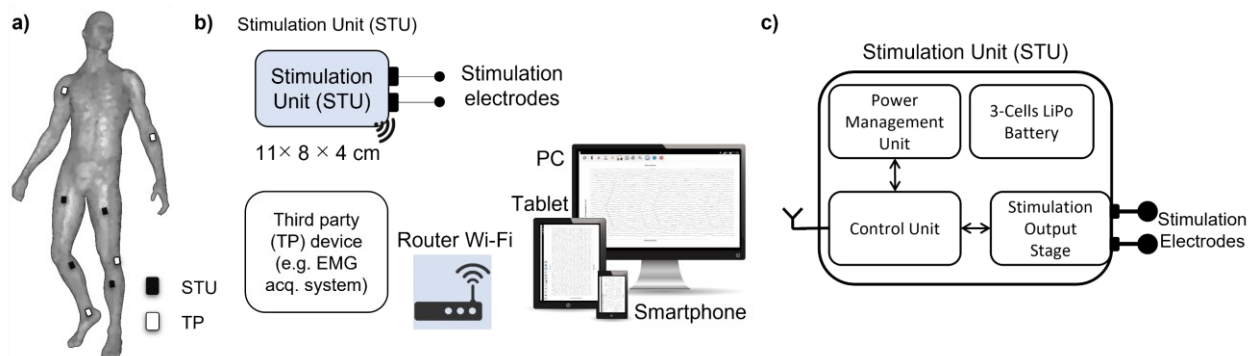
FIGURE 1. a) Representation of a wireless Body Sensor Network (wBSN) composed of a set of stimulation modules (STU) and third-party modules (TP) used to collect physiological and biomechanical variables. b) Block diagram of the proposed system architecture. One or more STUs communicate with a Server (PC, Smartphone, Tablet) through a Wi-Fi wireless link. Third party device(s) can be added to this network to ensure the possibility to acquire signals used as stimulation trigger source. c) Block diagram of the STU module. The Stimulation Output Stage delivers pulses to the subject and is controlled by the Control Unit. The Control Unit performs both the management of the wireless communication with the Server, and the trigger of the stimulation start/stop commands, together with basic safety controls. The Power Management Unit feeds the Control Unit and both the low-voltage and the high-voltage, isolated analog circuits of the Stimulation Output Stage. The system is powered by a 3-cells Lithium Polymers battery.

angles or external forces. Closed-loop stimulation would demand the use of external data acquisition devices. Specifically, regarding the concurrent stimulation multiple muscles, currently available devices rely mainly on multiplexing the output channels for ensuring a high number of stimulation channels. On one hand, multiplexing allows using a single output stage to deliver stimulation pulses to different muscles, with a different timing. On the other hand, multiplexing requires to physically connect the stimulation device to the different target muscles opening some issues in wearability and movement freedom (e.g. FES-Rowing and FES-cycling; [21], [22]), in particular if the outdoor use of FES is to be pursued [23] or muscles of different limbs must be stimulated. Indeed, using a monolithic solution would increase the complexity of the experimental setup because long wires are required to connect the stimulation unit to the stimulation electrodes, increasing the risk of improper/missed stimulation due to the possible disconnection of the connecting cables. Furthermore, designing multi-channel, monolithic stimulators with non-multiplexed outputs implies a relevant increase of the overall device size due to the required, galvanic isolation of each stimulation channel. Although the size of these devices would not represent a limitation in case of integration within large rehabilitation or gym equipment (e.g. for FES-cycling), this solution is overtly not viable for portable systems.

In this study, we propose a feasible solution for the closed-loop stimulation of multiple muscles. Here we describe the design of a neuromuscular electrical stimulator whose system architecture is characterized by i) modularity, ii) wireless communication, iii) ease of integration with third-party devices for the acquisition of external biomechanical/electrophysiological signals, iv) programmability of the stimulation patterns based on external signals, and v) scalability. The design was driven by both safety and performance optimization principles. To the best of our knowledge, a device complying with the aforementioned characteristics was not previously described in the literature. A preliminary description of the device presented here has

been summarized in a previous work [18]. Here we aim to describe in detail the design and test of the device as well as its validation in experimental protocols requiring the combination with other third-party devices for kinematic and surface EMG (sEMG) signal acquisition. Furthermore, this work presents the design of additional controls (e.g. voltage/current monitors) and features (e.g. programmability of a custom stimulation pattern based on sEMG envelopes) not available before.

II. SYSTEM DESIGN

A. SYSTEM ARCHITECTURE

Figure 1.a and Figure 1.b show the system architecture. The system is composed of a set of programmable, electric stimulation modules (Stimulation Unit, STU). The stimulation pattern of each STU can be driven by the server processing the signals coming from third-party devices.

The choice of using a modular, wireless, and de-centralized system architecture allows simplifying the experimental setup, dismissing the need for long cables for the electrode connection. This modular architecture makes the system usable in scenarios where both third-party sensors and stimulating modules are needed and during highly dynamic tasks (e.g. sport). Furthermore, the modularity allows to choose the number of stimulation channels (STU) depending on the specific application the stimulator is used for, thus allowing to optimize the total system encumbrance and consequently improve the overall system flexibility.

The STU is a wireless, programmable single channel electrical stimulator issuing either monophasic or biphasic current pulses with amplitude, frequency, and pulse duration settable by software. Multiple STU modules communicate either with PCs, mobile devices (Smartphone or Tablet) or a single board computer (e.g. Raspberry Pi) configured as a server. The software running on the server may be used to acquire signals from third-party sensors, to program the stimulation pattern on a channel basis, and elaborate acquired signals used as a trigger source to control the start/stop of the

stimulation. The software was indeed designed to ensure the acquisition of signals from different devices.

B. STIMULATION UNIT DESIGN

The STU is a wireless, programmable electrical stimulator issuing either monophasic or biphasic current pulses with amplitude ranging from 100 µA to 100 mA and voltage from -150 V to 150 V, depending on the impedance of the load to which the stimulation is issued. Stimulation frequency can be programmed from 0.1 Hz to 200 Hz at steps of 0.1 Hz whereas pulse duration may be set from 0.01 ms to 100 ms at 0.01 ms steps.

The STU is composed of three main blocks (Control Unit, Stimulation Output Stage, and Power Management Unit) as shown in Figure 1.c. The Control Unit is responsible for i) the wireless communication with the server, ii) the start/stop of the stimulation, iii) the control of the stimulation pattern and parameters, and iv) the management of safety controls. The Stimulation Output Stage is responsible for the delivery of current pulses and houses the safety control and all related circuits. The Power Management Unit feeds the Control Unit and both the low- and high-voltage isolated analog circuits of the Stimulation Output Stage. The system is powered by a 3-cells Lithium Polymers battery (11.1 V nominal voltage). The choice to design a battery powered device instead of a mains-powered device is mainly due to the wearability requirement of the proposed system and improves the overall safety of the device, since it reduces the risk associated with possible leakage currents injected into the subject from the device applied parts (i.e. the electrodes connection and the stimulation output stage) coming from the 50 Hz/60 Hz mains [24].
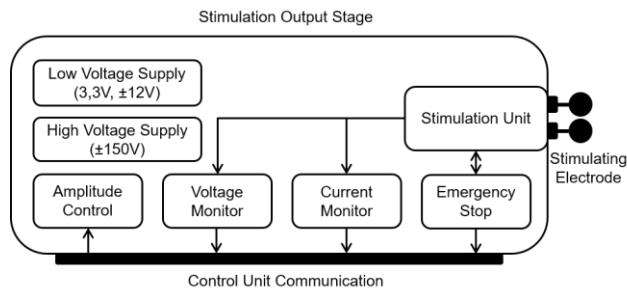
C. STIMULATION OUTPUT STAGE

The Stimulation Output Stage provides current pulses following a user-defined pattern. The choice of issuing current pulses instead of voltage pulses was due to the inevitable variations of tissue impedance following a square pulse having high frequency components [25]. A hybrid output stage [19], [26] was designed to reduce the stimulation artefact detected by devices acquiring biopotentials (e.g. sEMG) on the skin. Within this stimulation scheme (Figure 2.a), the output stage switches between a constant current stimulator during ON periods (the active phases of the stimulation) and a low impedance path between electrodes during OFF periods (the quiescent phases of the stimulation), reducing rapidly the residual load voltage at the electrode-skin interface (Figure 2.b) and thus the stimulation artefact (Figure 2.b). Furthermore, the low-impedance path during the quiescent phase of the stimuli further suppresses the accumulation of a net charge at the electrode-skin interface when monophasic pulses are used as demonstrated by the fact that no residual voltage is observed in Figure 2.b after the short circuiting of the electrodes. Indeed, it is well known that, if the net charge transferred to the patient is different from zero, then ions at the electrode-skin interface could lead to the formation of acids at the interface, with consequent stimulation-induced side effects such as chemical burns or skin irritation [27], [28].

Figure 3 shows the block diagram of the Stimulation Output Stage. It is composed of five main circuits: a high voltage transconductance amplifier (Stimulation Unit), an amplitude control circuit, voltage and current monitors, and an emergency stop circuit. Three isolated supply voltages (3.3V, ±12V, ±150V) power the amplitude control/emergency stop circuits, the voltage/current monitors, and the Stimulation Unit, respectively. The choice to power the Stimulation Unit with a high DC voltage is due to the need to inject a relatively high current (up to 100 mA in this case) into an impedance load (i.e. the electrode-skin-muscle system) of up to few kilo-Ohm. Consequently, safety-related problems need to be carefully addressed, designing redundant safety measures and circuits (e.g. hybrid stimulation scheme, voltage and current

$$\tau_1 = R_P C_P \qquad \tau_2 = (R_P \oplus R_S)C_P \approx R_S C_P \leftrightarrow R_P \gg R_S \qquad \tau_1 \gg \tau_2$$
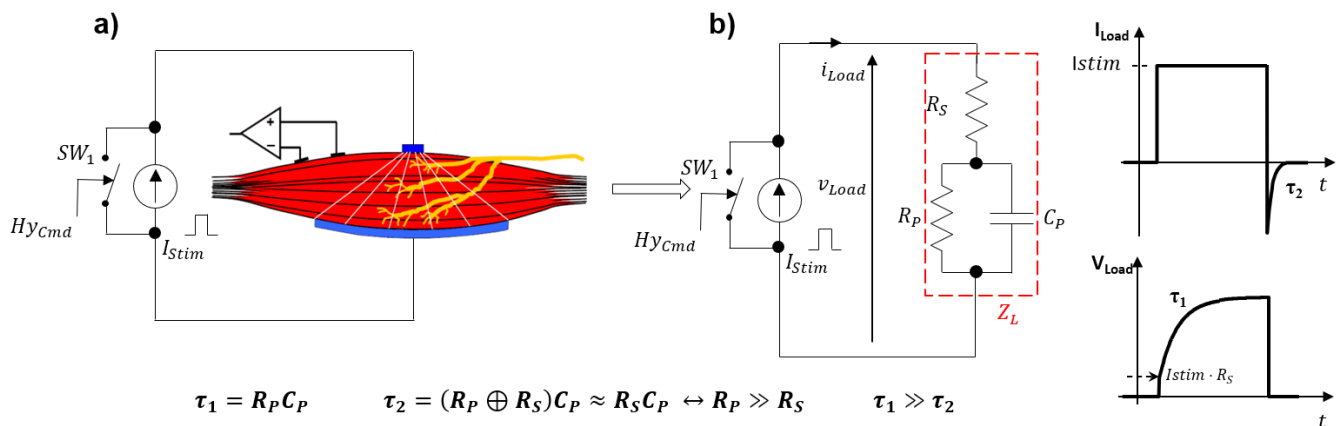
FIGURE 2. a) Schematic representation of a hybrid stimulation output stage. It can be considered as a constant current generator during the active phase of the stimulation and a short circuit during its quiescent phase. HyCMD drives the switching between the ON and OFF state of the stimulation. Electrical equivalent circuit representing the interaction between the hybrid output stage and the electrodes. The electrode-skin interface is modeled as a R-C circuit. The voltage and current time courses following a stimulus are represented. During the ON phase of the stimulus, the proposed circuit acts as a current source, while during the OFF state of the stimulus it acts as a voltage source, quickly extinguishing the residual voltage at the electrode-skin interface.
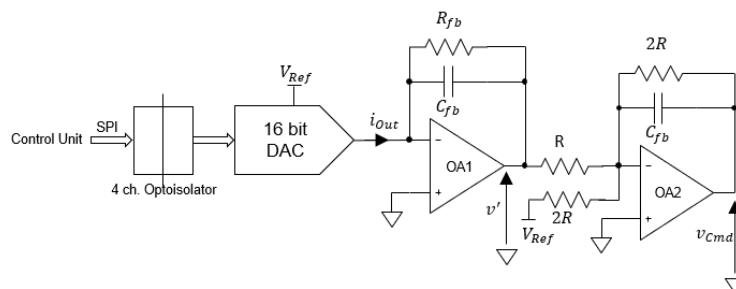
FIGURE 3. Block Diagram of the Stimulation Output Stage. The Stimulation Output stage is fed by three different power supplies (3.3V, ±3.3V e ±150V). The Amplitude Control block allows to set the current amplitude of the stimulation, the voltage and current monitors allow to control, through the Control Unit, the voltage and current over the load during the stimulation. The Emergency Stop circuit allows to short-circuit the load in case of fault conditions or to provide a fast discharge path for the residual voltage after the stimulation. The Stimulation Unit is a programmable constant current generator that provides stimulation pulses to the subject.

monitors, isolated battery power supply) able to mitigate possible faults of the Stimulation Unit.

The amplitude control circuit (Figure 4) sets the current stimulation level regulating the V_{CMD} voltage and consequently drives the transconductance amplifier. It is composed of the DAC8811 (Texas Instruments, USA), 16bits, R-2R Digital-to-Analog Converter (DAC) and a transconductance amplifier (needed to convert the DAC's current output to a voltage signal used to drive the stimulation unit) and a low-pass filter (f_c=1.6 MHz, Gain=6 dB) in series used to reconstruct the output signal and avoid spurious interference due to e.g. radio-frequencies or wireless communications. The stimulation unit is driven either with positive or negative voltages, thus allowing to obtain biphasic current pulses. To allow the stimulation unit to be driven either with positive and negative voltages and consequently permit the formation of biphasic current pulses, a voltage reference of 1.65 V (V_{REF}) was added to the transconductance amplifier (v' = $i_{Out}Z_{fb}$, where Z_{fb} is the impedance given by R_{fb}//C_{fb}). The voltage at the output of the amplitude control circuit (V_{Cmd}) is given by (1).

$$V_{Cmd} = 2i_{Out}Z_{fb} - V_{REF} \qquad (1)$$

The DAC communicates with the Control Unit through a standard SPI peripheral isolated through the quad-channels digital isolator ADUM2401ARWZ (Analog Devices, USA).
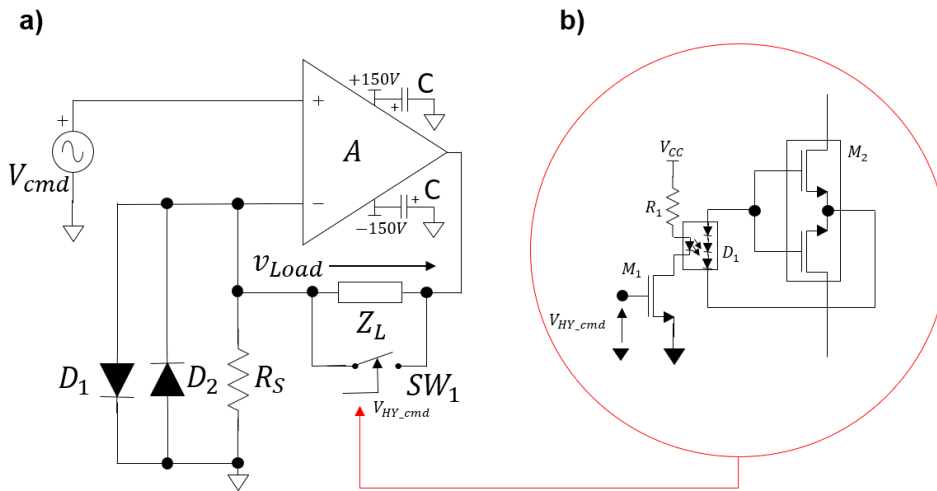
In this way, the stimulator output stage is galvanically isolated from the control unit, thus reducing the risk of unwanted electric shock given to the operators.

The designed amplitude control circuit allows giving biphasic current pulses with 100 mA$_p$ with a theoretical resolution of 3µA.

The high voltage transconductance amplifier (Figure 5) uses the PA78DK (Apex Microtechnology, Arizona, USA) power operational amplifier and converts voltage pulses given by the amplitude control circuits, as provided by the microcontroller, into current pulses. The PA78DK was chosen for the high output voltage range (±175 V), Gain-Bandwidth Product (GBP – 1 MHz) and Slew Rate (350 V/µs). The transconductance amplifier was set with R_s=16 Ω in order to have a current of 100 mA$_p$ with an input signal of 1.6 V$_p$. The load current at the output of the transconductance amplifier results:

$$I_L = \frac{V_{CMD}}{R_S} \qquad (2)$$

Two diodes (D$_1$-D$_2$; Figure 5) were obtained by connecting three diodes with V$_\gamma$=1.2 V in series, limiting the input voltage to the transconductance amplifier and thus the maximum current injected into the load to around 220 mA$_p$, also during possible faults of the control circuits. The PA78DK is powered by a ±150 V DC power supply discussed in the Power Management Unit Section.

FIGURE 4. Shematic diagram of the amplitude control circuit. It is composed of: DAC8811 (Texas Instruments, USA), 16bits, R-2R Digital-to-Analog Converter (DAC) and a series of a transconductance amplifier and a low-pass filter (fc=1.6 MHz, Gain 6dB). The DAC input signals are isolated from the Control Unit through a standard quad-channels digital isolator.

This article has been accepted for publication in a future issue of this journal, but has not been fully edited. Content may change prior to final publication. Citation information: DOI 10.1109/ACCESS.2021.3133096, IEEE Access

IEEE *Access* Cerone et al: Design of a programmable and modular neuromuscular electrical stimulator integrated into a wireless Body Sensor Network

FIGURE 5. a) Schematic principle of the Stimulation Unit. It is composed of a transconductance amplifier based on the PA78DK (Apex Microtechnology, Arizona, USA) power operational amplifier. Rs was set to have a maximum stimulation current of 100 mAp with an input signal of 1.6 Vp. The residual load voltage (VL) at the end of the stimulation can be reset by means of the electronic switch SW1 that represents the simplified Emergency Stop circuit (b). Diodes D1-D2 have been used as a safety measure to limit the input voltage of the transconductance amplifier and thus, the maximum current injectable into the load. The circuit is powered by a ±150V DC power supply. b) Schematic detail of the Emergency Stop Circuit. It was designed using two power N-MOSFETs (M2) connected source-to-source. The photovoltaic MOSFET Driver (D1) and the M1 MOSFET provide galvanic isolation from the Control Unit and drive M2 respectively.

The emergency stop circuit (Figure 5.b) short-circuits the load between the electrodes during the quiescent phase of the stimulation (i.e. between two current pulses), thus creating a low impedance path between the stimulation electrodes. It is driven by a digital command coming from the Control Unit. This circuit has two purposes: i) to stop the stimulation pulse in case of dangerous conditions (e.g. the stimulation is applied for a long period), ii) to rapidly discharge the post-pulse charge, thus reducing the stimulation artefact [26]. The short-circuit of the load is obtained through a dual N-MOSFET (M_2) in which the internal MOSFETs are connected in the source-

to-source configuration. The common gate drives the short-circuit command provided by the Control Unit (V_{HY-CMD}). The FW276 (On Semiconductor, USA) dual N-Type MOSFET has been chosen to guarantee the functioning of the circuit over the entire output range (±150 V) of the stimulator module. It has a maximum Drain-to-Source voltage (V_{DS}) of 450 V and a Gate-to-Source voltage (V_{GS}) between 3.5 V and 4.5 V. The FW276 chip is driven by the VOM1271 (Vishay Semiconductors, USA) photovoltaic MOSFET Driver (D_1 in Figure 5.b) that provides also galvanic isolation between the High Voltage Stimulation Unit and the Control Unit. The M_1
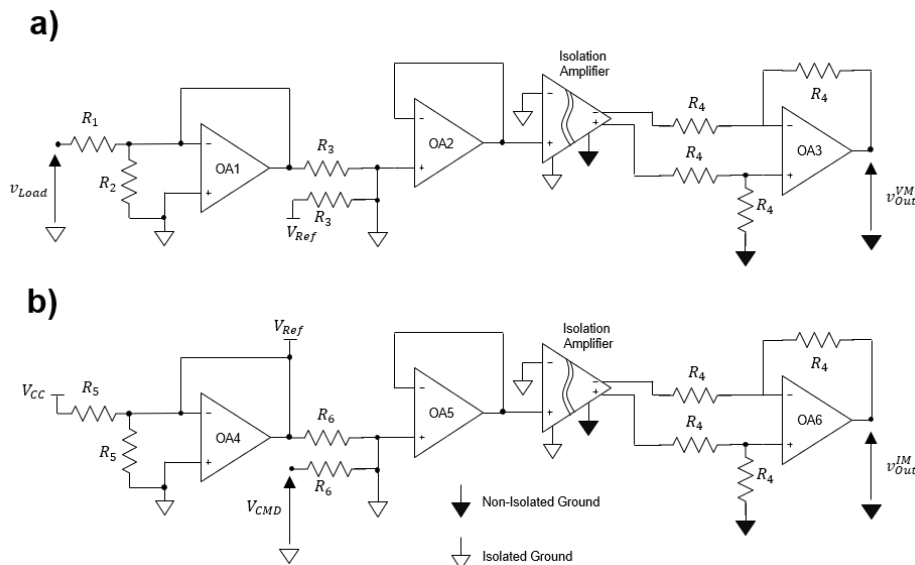
FIGURE 6. Schematic diagram of the Load Voltage (a) and Load Current (b) monitor circuits. a) The voltage monitor is composed of a voltage divider (R1, R2), a buffer with a +1.65V offset allowing the microcontroller to sample positive and negative signals. b) The current monitor is composed of a buffer to sum the voltage at the input of the stimulation output stage (VRS) to a +1.65V offset used to allow the microcontroller to sample positive and negative signals. Both the signals are isolated with respect to the Control Unit through a fully differential analog isolation amplifier and a non-isolated differential amplifier (G=1V/V). The isolated power supply is fed by the ±3.3V Step-Down DC/DC converter.

MOSFET drives the VOM1271 on the basis of a digital command coming to its gate from the Control Unit.

The simplified circuit diagram for the Voltage (VM) and Current (IM) monitors are shown in Figure 6.a and Figure 6.b, respectively. VM and IM allow the Control Unit to sample (fs = 1 kHz, 12 bits resolution) signals proportional to the current and voltage flowing into the load under stimulation. These circuits provide an additional safety measure because they allow to digitally verify the absence of unpredictable dangerous conditions (e.g. high DC voltages) due either to bugs, hardware malfunctioning, hardware fails, or inappropriate programming/use. It is possible to define specific, possibly dangerous, conditions that must be monitored (e.g. event of uninterrupted electrical stimulation) and stop the stimulation through a command sent by the Server or through the emergency stop circuit. The voltage and current monitors allow also to calibrate the DAC with a known, embedded resistive load (R_L = 1 kΩ) to mitigate offset and gain errors. Due to the relatively short duration of the current pulses (hundreds of micro-seconds) and to the low sampling frequency selected, it is not possible to real-time monitor the voltage and current pulses shape and this explains why VM and IM were used as additional control measures and not as primary safety measures.

The voltage monitor is composed of a voltage divider (R_1, R_2), which limits the high voltage of the load (±150 V) into the low-voltage rails (±3.3 V) of the Control Unit, and a buffer with a +1.65 V offset (V_{Ref}) used to allow the sampling of both positive and negative phases of the stimulation pulses.

The current monitor is driven by the stimulation input voltage V_{CMD}, which is proportional to the current flowing into the load according to (2). A buffer adds +1.65 V offset (V_{Ref}) to V_{CMD} to allow the microcontroller to sample either positive and negative signals.

In both cases of voltage and current monitoring, a dedicated AMC1100 (Texas Instruments, USA) fully-differential isolation amplifier isolates the output signals from the Control Unit. The non-isolated differential amplifier (G=1V/V) is placed at the monitor's output to transform differential signals at the output of the AMC1100 isolation amplifier into single-ended signals.

According to Figure 8, the voltages at the voltage and current monitor outputs are defined by the following equations:

$$V_{Out}^{VM} = v_{Load} \frac{R_2}{R_1 + R_2} + 1.65V;$$

$$V_{Out}^{IM} = V_{CMD} + 1.65V \quad (3)$$

V_{Load} is the voltage on the load during the active phase of the stimulation and V_{Cmd} is the voltage driving the stimulation output stage.

C. CONTROL UNIT

The Control Unit implements i) the control of the stimulation pattern, ii) the wireless communication with the server, and iii) the sampling of current and voltage monitor outputs.

Considering that only Wi-Fi and Bluetooth natively support mobile devices, the Wi-Fi transmission protocol was preferred to achieve the possibility to connect more than 7 stimulation modules at the same time. The Texas Instruments CC3200 system-on-chip wireless MCU was selected. The wireless MCU integrates an ARM Cortex-M4 MCU core (Main Processor, MP) running at 80MHz and an additional dedicated ARM MCU (Network Processor, NWP) that acts as a Wi-Fi network processor subsystem including an embedded TCP/IP stack. The NWP manages the Transport (TCP), Network (IP) and Physical layers of the TCP/IP model applied to the Wi-Fi protocol and uses a standard BSD Socket implementation as Application Programming Interface (API). This feature limits the tasks performed by MP to i) stimulation pattern control and data sampling and ii) management of the application layer of the transmission protocol. The Control Unit firmware was written in C language. The CC3200 microcontroller integrates a real-time operating system (FreeRTOS) and runs three different parallel tasks: i) Wi-Fi communication, ii) data sampling, and iii) control of the stimulation pattern and, optionally, of the waveform shapes that are digitally programmable through the software running on the Server.

The Wi-Fi communication task allows each stimulation module to communicate with the Server, to receive a user-defined stimulation pattern (programmable in terms of amplitude, stimulation pattern, duration, and frequency of the stimulation), to receive the start/stop of the stimulation, and to send to the server status messages.

The data sampling of current and voltage monitors (f_s=1 kHz) is carried out in a separate task using the 4-Channels, 12 bit internal A/D converter. The stimulation is controlled by a dedicated finite-state task that controls the DAC of the stimulation output stage and runs the user-defined stimulation pattern following a specific server command (e.g. stimulation start/stop).

C. POWER MANAGEMENT UNIT

The stimulation module has three main power supply voltages (3.3 V, ±3.3 V, and ±150 V) that feed the Control Unit and both the low-voltage and the high-voltage isolated analog circuits of the Stimulation Output Stage. The Control Unit power supply is given by a 3.3 V Step-Down DC/DC Converter (TPS62160, Texas Instruments, USA) whereas the low-voltage, isolated power supply is given by an isolated, ±3.3 V step-down DC/DC converter (IA1203S, XP Power, Singapore).

The high voltage, isolated, power supply is given by the ±150 V ERG E712-3.010 (ERG Power, USA) isolated step-up DC/DC converter. The ripple at the output of the DC/DC converter is filtered by means of two 47 μF electrolytic

capacitors connected in anti-series (maximum D.C. voltage of 350 V).

III. SYSTEM PROTOTYPING

Three Stimulation Unit modules have been prototyped (Figure 7.a). The stimulation unit consists of two different PCBs: one for the Stimulation Unit and one for the Control Unit. The Stimulation Unit PCB is composed of a two-layer, 1 mm thick Printed Circuit Board (PCB) with components mounted on one side whereas the Control Unit is a 3 cm x 2 cm, 0.8 mm thick PCB designed also for the device described in [29]. The design was kept as simple as possible using only Commercially available Off-The-Shelf (COTS) components. The circuit prototypes have been mounted and encapsulated in a 3D printed case (Figure 7.b). The total encumbrance of a single STU module is 11 cm x 8 cm x 4 cm (thickness). The STU weight is 350 g of which 140 g is due to the integrated 3-cells LiPo battery. The size of the proposed device could have been lower by increasing the component density on the PCB and selecting components with smaller footprints. However, we preferred to avoid stressing the miniaturization requirements to reduce production costs, and facilitate bench tests, while keeping the requirement on the STU module portability.

IV. SOFTWARE DESCRIPTION

The software runs on the server (PC, Smartphone or Tablet) and communicates with the connected STU modules. It was developed using the Qt multiplatform C++ framework. The Graphical User Interface is composed of a control window for each connected module. This interface allows for the real-time visualization of data acquired with third-party devices (e.g. [18], [30]), the programming of STUs with user-defined patterns, and the control of the stimulation triggering of the stimulation (start/stop). The programmed stimulation pattern is coded by two vectors defining the mutual combination between stimulation amplitudes and time intervals. For instance, a monophasic current pulse of 30 mA lasting 100 µs and repeated at 20 pps is coded by the software with the following vectors: [30;0] (amplitude vector expressed in mA); [0.1;49.9] (time vector expressed in ms). The user defines the stimulation parameters through a simple Graphical User Interface (GUI) allowing to set the stimulation amplitude, period, and frequency. The codification is synthesized automatically by the Software. This approach allows to synthesize arbitrary waveforms, not necessarily based on square pulses, and can be generalized to the case in which the synthesis of the stimulation pattern is based on the features of signals recorded from third-party devices (as shown in Section VI.A). Indeed, the software allows basic real-time pre-processing of the acquired signals: DC-removal, signal rectification, calculation of sEMG ARV, RMS, and envelopes. Stimulation patterns may be defined by the user or on the basis of the control signal features (e.g. sEMG envelope). The stimulation output can be triggered either directly or through

analog signals sampled by other acquisition systems, allowing closed-loop stimulation protocols [15], [16].

V. SYSTEM CHARACTERIZATION

A. STU CHARACTERIZATION

The Stimulation module has been characterized in terms of stimulation output stage performances, and power consumption. The wireless link performances do not constitute a critical aspect within this application context thanks to the extremely low data throughput required by the system. Indeed, the communication between the Stimulation Unit and the receiver is needed only during the programming of the stimulation pattern and to start/stop the stimulation. Considering this fact and the maximum number of connected devices supported by the Wi-Fi network (256), it is clear that the wireless link does not represent a limitation on the number of STUs that can be connected at the same time.

B. STIMULATION OUTPUT STAGE

The stimulation output stage was bench-tested using a 1 kΩ resistive load and varying the stimulation pattern in terms of current amplitude, frequency, and duration of the stimulation. Considering the switching noise due to the high voltage DC/DC converter, the minimum current step between two different stimuli was increased to 100 µA instead of the 3 µA theoretically calculated (i.e. the current step corresponding to a one-level increment of the DAC output). This result does not affect the overall performances of the electrical stimulator module and is therefore acceptable for the aim of the work. The stimulation output voltage between anode and cathode of the stimulator was measured through an oscilloscope (MSO-X-2024A, Texas Instruments, USA) programming the stimulator to provide monophasic stimuli (100 mA, 300 µs, 10 Hz). The measured rise time for a 100 mA current pulse over a 1 kΩ resistive load was less than 10 µs. The 1 kΩ load was chosen because it approximates the electrode-skin impedance for standard carbon electrodes (16 cm^2 surface) used for electrical stimulation [31]. The measured rise time results of great interest because a high slope of the stimulation output ensures an almost constant transfer of electrical charge, resulting in a high repeatability of the stimulation pulses.
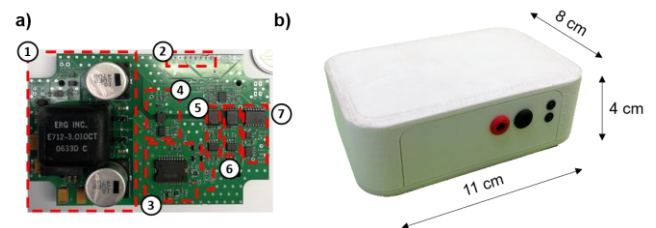
FIGURE 7. a) Printed Circuit Board of the Stimulation Unit prototype. The two layers, 1 mm thick, PCB has the components mounted on one side. The main blocks constituting the STU module are indicated: 1) Power Management Unit; 2) Control Unit connector. The Control Unit was developed in [29]; 3) Stimulation Unit; 4) Emergency Stop; 5) Voltage Monitor; 6) Current Monitor; 7) Amplitude Control. b) Stimulation Unit prototype boxed into a 3D printed case.

The emergency stop circuit, used as a low impedance discharge path for the residual charge following a stimulus, was tested providing a 100mA current pulse over a known impedance of 1 kΩ and measuring the voltage falling time over the load. The resulting falling time was less than 1 μs in the worst-case condition. These results confirmed that the Stimulation Unit acts as a current generator with relatively high source impedance during the active phase of the stimulation and as a low-impedance path during the quiescent phase. The current stimulus is transferred to the subject's skin with negligible current leakages (< 50 μA_{RMS} in the bandwidth between 0 Hz and 1 kHz) through the stimulator source impedance. For this reason, the electrical charge transferred to the subject can be considered constant and repeatable among different stimuli.

C. POWER CONSUMPTION

The system has been powered by a three cells LiPo Battery Pack (Il Ricaricabile, Torino, Italy) with a nominal voltage of 11.1 V and a capacity of 2.6 Ah. The ripple on the high-voltage power supply resulted in around 12 mV_{RMS} (0.5 V_{pp}). The system power consumption was measured using two true RMS multimeters configured as voltmeter and ampere-meter, respectively. The battery voltage (V_{Bat}) and the battery output current (I_{Bat}) were measured. The power consumption ($P = V_{Bat} I_{Bat}$) resulted around 2 W and is mainly due to both the Wi-Fi (0.3 W) and stimulation output stage power consumption (1.5 W). Different current stimuli waveforms and programmed patterns can be neglected in the power consumption estimation because, due to their short duration, the mean power transferred to the load is usually below a few tens of mW.

Given the capacity of the battery, the Stimulation Unit has an expected battery life of 13 hours comparable to that of the Sensor Unit modules designed in [18]. Considering this relatively long battery life, reducing the capacity of the battery could be a feasible choice for future re-designs aimed at reducing the overall size and weight of the device.

VI. EXPERIMENTAL TESTS

The experimental validation was aimed to demonstrate the capabilities of the proposed device in real world scenarios. In order to show the device's main features (modularity, programmability of the stimulation pattern, and communication with third party devices), we designed two FES cycling protocols requiring two stimulation modules and two external devices.

Each experimental protocol was applied to one healthy subject (27 years, 76 kg, 180 cm). The study was conducted in accordance with the Declaration of Helsinki and the informed consent was obtained from the participant after receiving a detailed explanation of the study procedures.

Both experimental protocols involved the sEMG-driven stimulation of the leg muscles and the synchronized recording of the knee angle. The first study ("contralateral control of leg extension") illustrates the technical feasibility to control a supposed paretic limb through the replication of the activation intervals of the contralateral, healthy, limb during cycling. Specifically, sEMG signals were collected from the right quadriceps (RQ) and tibialis anterior (TA) muscles, and a time-shifted version of their activation intervals was used to stimulate the correspondent muscles of the left leg. In the second study ("sEMG control of lower limb"), sEMG signals from biceps and triceps brachii were used to respectively stimulate the left and right knee extensors, without any delay other than that associated with data transmission. The experimental details and the results of both studies are described in the following sections.

It is worth noting that these experiments were sought with the sole purpose of showing the adequacy of the proposed system in closed-loop FES applications. Inferences on the physiological mechanisms underpinning the closed-loop stimulation or on the potential, applied benefits of this system are not intended here.

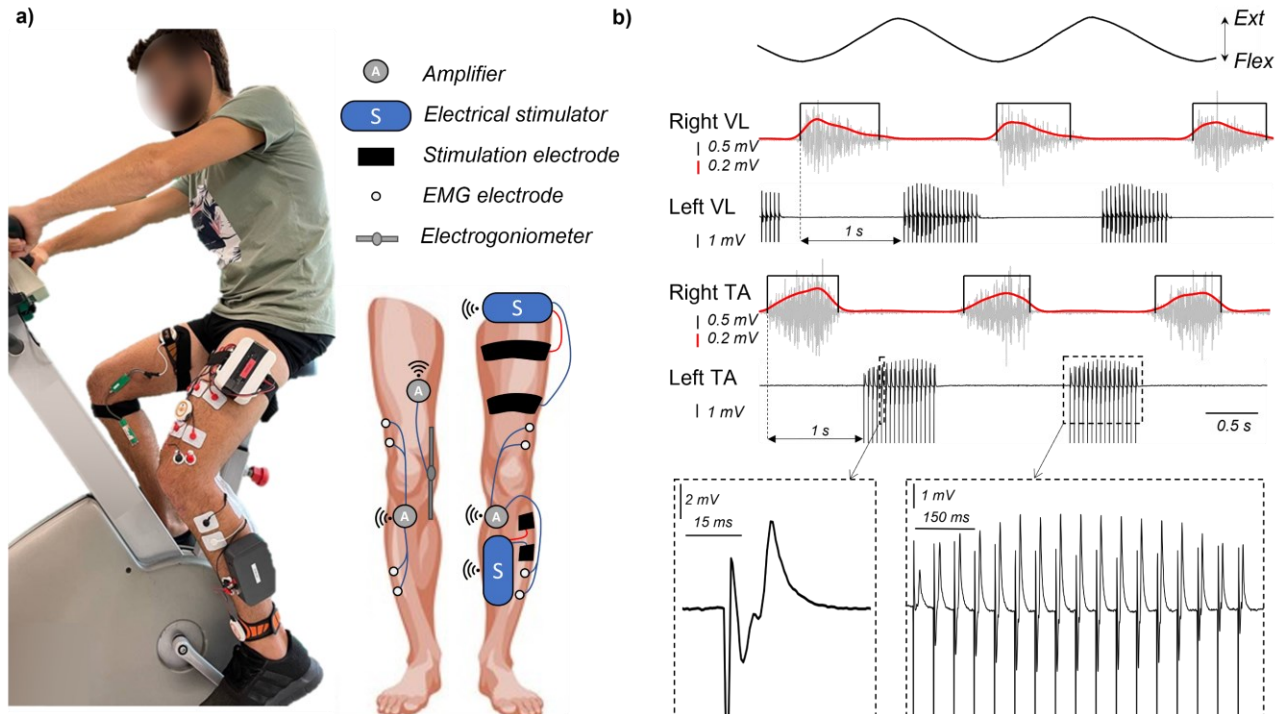### A. CONTRALATERAL CONTROL OF LEG EXTENSION

The experimental setup adopted in this study is depicted in Figure 8.a. Two STU modules have been programmed to stimulate the left Quadriceps and TA muscles with a monophasic current pulse (20 mA - 50 mA based on the amplitude of the contralateral sEMG signals, 100μs, 20 pps). Two 5 cm x 4 cm adhesive stimulation electrodes (SpesMedica, Battipaglia, Italy) were positioned on the proximal (cathode) and distal (anode) TA regions according to motor point positions [32]. For quadriceps stimulation, three cathode and three anode electrodes (5 cm x 4 cm each, SpesMedica, Battipaglia, Italy) were short circuited and positioned according to [33], maximizing the knee extension torque. Bipolar sEMG signals were collected from the Vastus Lateralis (VL) and TA muscles of both legs with pairs of adhesive electrodes (Kendall, CardinalHealth, USA, IED = 2 cm). Detected signals were amplified with a wireless sEMG acquisition system (Due, OT Biolettronica, Torino, Italy). Knee joint angle was measured throughout the cycling task with an electro-goniometer (SG110, Biometrics Ltd, Newport, UK) connected to a wireless acquisition system (DuePro, OT Biolettronica, Torino, Italy). The subject was instructed to exercise at a light, fixed pace (30 rpm) while voluntarily moving only the right leg. Stimulation of knee extensors and the TA muscles in the left leg was then triggered based on the activation interval of their paired, contralateral muscles. The amplitude of the stimulation pulses was automatically adapted in the range 20 mA – 50 mA by the software, based on the envelope amplitude of the collected sEMG signals. Activation intervals were extracted by setting a single threshold on sEMG envelopes computed in real time from the right limb muscles (2nd order Butterworth low-pass Filter, $f_c = 1$ Hz). The extracted intervals were delayed by 1 s and used to trigger the sEMG-driven stimulation of the contralateral muscles.

Figure 8.b shows the knee angle and sEMG signals detected during four cycles. Voluntary activation of right leg muscles during the knee extension phase (VL) and around the maximal flexion phase (TA) can be observed (light gray traces in Figure 8.b). As programmed, the stimulation intervals of left VL and TA are the time shifted (1 s) versions of the activation intervals computed from right VL ad TA respectively. Stimulated signals (black traces in Figure 8.b) show the typical temporal sequence of stimulation artifact, indicating the stimulation onset, followed by the M wave after few milliseconds [34]. Dashed panels in Figure 8.b show the detail of a single M wave and a M-waves burst with amplitudes following the sEMG envelope profile. No voluntary EMG activity was observed in both stimulated signals, suggesting the main contribution of the electrical stimulation to the knee joint kinematic (upper black trace in Figure 8.b). Regarding the knee angle profile, it is overtly highly dependent on the delay selected for issuing the train stimulation pulses after the activation interval has been identified in the contralateral limb. In the limit case of no delay, for example, movement of both legs would likely be greatly hindered, given that knee extensors and ankle dorsiflexors in both legs would be excited concurrently. After few attempts, we observed the tested subject could readily cycle at the requested 30 rpm pace with a 1 s delay. The smooth knee angle profile shown in Figure 8 substantiates this observation, as the validity of the system in terms of modularity, programmability, and communication with third-party devices.

B. sEMG CONTROL OF LOWER LIMB

Figure 9.a shows the second experimental protocol. Two STUs have been programmed to stimulate the right and left quadriceps with monophasic stimuli (50 mA, 100μs, and 20 pps). Three cathode and three anode electrodes (5 cm x 4 cm each, SpesMedica, Battipaglia, Italy) were short-circuited and positioned on both quadriceps as indicated in the previous experiment. Bipolar sEMG signals were collected from the VL and Vastus Medialis (VM) muscles of both legs with pairs of adhesive electrodes (Kendall, CardinalHealth, USA, IED = 3 cm) and using two sEMG probes having two acquisition channels each (Due, OT Biolettronica, Torino, Italy). Bipolar sEMG signals from the Biceps Brachii (BB) and Triceps Brachii (TB) muscles were acquired using a third sEMG acquisition module and served as input signals for the triggering of the stimulation pattern. The right knee joint angle was measured throughout the cycling task with an electro-goniometer (SG110, Biometrics Ltd, Newport, UK) connected to a general-purpose wireless acquisition system (DueBio, OT Biolettronica, Torino, Italy). The subject was instructed to exercise at 30 rpm and to avoid the voluntary knee extension. The start and end of stimulation of the right and left knee extensors were triggered by the onset of activation and silencing of BB and TB, respectively. Onsets were extracted

FIGURE 8. Example of a potential, FES-Cycling application: contralateral control of leg extension. a) Experimental setup including: a wireless acquisition system for the right knee joint angle, two wireless sEMG acquisition systems for both left and right VL and TA muscular activity, two STU modules on the left leg programmed to stimulate left VL and TA. STU modules replicate the activation of the right muscles on the respective contralateral ones with 1-s time delay by modulating the stimulation amplitude according to the voluntary sEMG envelopes of the right muscles (see signals in panel b). b) Knee angle and sEMG signals detected during two pedaling cycles: knee joint kinematic, raw sEMG signals (light grey) and their envelopes (red) from right leg muscles showing muscle activation during the knee extension phase (VL) and around the maximal flexion phase (TA), and the corresponding, stimulated signals from left VL and TA (black traces).
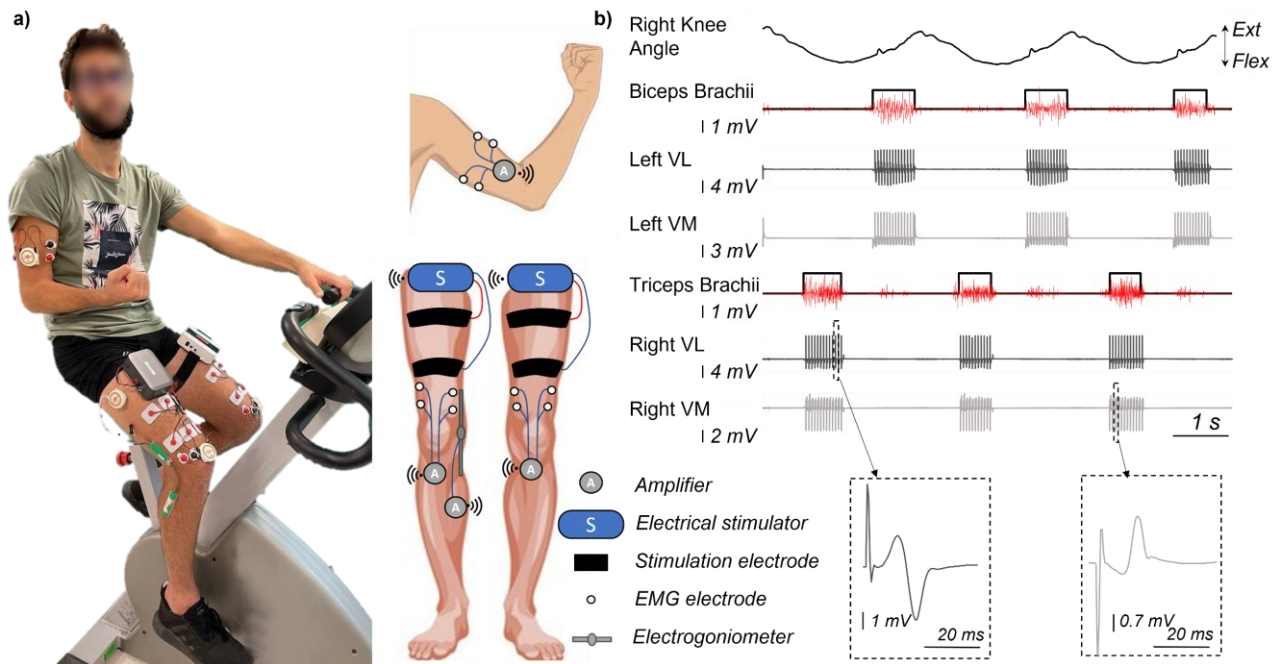
FIGURE 9. Example of a potential, FES-Cycling application: sEMG control of lower limb. a) Experimental setup including: a wireless acquisition system for the right knee joint angle, two wireless sEMG acquisition systems for both left and right VL and TA muscular activity and one for right BB and TB muscular activity, two STU modules on both legs (VL and VL muscles). Stimulation of the right and left knee extensors was triggered by the muscular activation intervals of BB and TB, respectively. b) Knee angle and EMG signals detected during four pedaling cycles: knee joint kinematic (black trace), voluntary activations of BB and TB (red traces), signals from stimulated left and right VL (dark grey traces) and from left and right VM (light grey traces).

by applying a single threshold on the BB and TB sEMG envelopes computed in real time (2nd order Butterworth low-pass Filter, f_c = 1 Hz). No delays between the trigger signal and the stimulation onset have been added, other than that associated with wireless data transmission latencies.

Figure 9.b shows the knee angle and sEMG signals detected during four cycles. It is important to note that a delay of 40 ms ± 2 ms was observed between the onset of the sEMG trigger signals and the stimulation artifact produced in the contralateral, elicited, muscle. This result may be essentially due to two factors: i) the intrinsic latency introduced by the wireless communication between the STU/acquisition systems and the Server, ii) the filter parameters chosen to calculate the sEMG envelopes. The latter factor is not discussed here as it does not fit with the aim of this work. Regarding the hardware delays, most of the latency (32 ms) was introduced by the sEMG acquisition system and corresponded to the length of the data packet transmitted from the sEMG probe to the Server. Therefore, the entity of the delay depends on the acquisition system used to drive the stimulation. Considering the setup used here, the smooth angle profile shown in Figure 9.b documents the validity of the system in closed-loop applications. Even though the subject was instructed to do not voluntarily control his legs, it is not theoretically possible to discard the contribution of other muscles to the leg movement after having detected EMGs only from the two superficial vastii muscles. Being VL and VM two main knee extensor muscles, however, the absence of motor unit action potentials within the stimulation period (Figure 9.b) evidences a major contribution of electrical

stimulation of these muscles to the extension and flexion phases of the movement.

Collectively, the two experiments just described indicate the stimulation device proposed here meets the technical requirements for different, application scenarios.

VII. CONCLUSION

This paper described the design of a modular, wireless, and programmable multi-channel electrical stimulator especially developed for FES and real-time applications. The system architecture and the main design choices, including safety concerns, were discussed. The hardware design was focused on conciliating high performance in terms of features of the stimulation pulses together with a high degree of safety for the subject. The flexibility of the proposed system architecture allowed to interface the system with third-party acquisition devices used to acquire trigger signals and validate the system. The possibility of the developed device and related software to interface with third-party biomedical instrumentation allowed the contemporary acquisition of sEMG signals used as trigger source for the electrical stimulation onset and offset.

The presented study used the Due bio-signal acquisition system (OT Bioelettronica, Italy) as its communication protocol is open access, thus allowing its integration into our system architecture. However, the proposed system architecture may be used with any third-party device, provided the availability of the communication protocol. Nevertheless, it is important to note that, when third-party devices are used as a source of stimulation trigger, particular attention has to be

taken because of the latencies and inter-modules synchronization delays introduced by the wireless transmission of such signals, as well as the quality of the collected signals. Potential synchronization issues between STU modules and third party devices need to be addressed on a case-by-case analysis, depending on the particular experimental setup and performance to be achieved. In this regard, care must be taken in the choice of the third-part devices when low latencies and high synchronization between the triggering of the stimulus and collected signals are required. In such cases, the adoption of the proposed device still results possible, but it is suggested to use a synchronization strategy as proposed in [35]–[37].

The experimental validation demonstrated the effective functioning of the proposed device in applied scenarios. Considering the actual device size and weight, the use of several modules may partially reduce the overall wearability of the proposed solutions. However, the experimental setup optimization such as placing the STU module in the proximity of the stimulation site (e.g. to the waist in case of stimulation of the thigh muscles) may partially mitigate this problem. Future improvements and developments may be focused on reducing the overall size of the Stimulation Unit, preserving the current features and performance. Beside the reduction of the battery size (see Section V.c), and a new PCB design oriented to the miniaturization of the board, a possible, innovative approach aimed to this end would be designing a rigid-flexible PCB integrated into textile garments. This approach would allow adapting the STU shape to different stimulation sites, improving the overall wearability of the device.

The specific design of the stimulation output stage, together with the system flexibility, modularity, and programmability represents an advancement of the State-of-the-Art technology in this field and constitutes a promising technological framework for the design of innovative devices for specific purposes (e.g. post-surgery rehabilitation, restoration of walking, FES-based rehabilitation, etc.) and for the definition of new protocols and treatments based on neuromuscular electrical stimulation.

VIII. CONFLICT OF INTEREST

DP and MI, are affiliated to CIONIC Inc. a Company developing and producing electrical stimulators for the drop foot correction.

ACKNOWLEDGMENT

REFERENCES

[1] N. A. Maffiuletti, "Physiological and methodological considerations for the use of neuromuscular electrical stimulation," *European Journal of Applied Physiology*, vol. 110, no. 2. 2010.

[2] E. F. Hodson-Tole, I. D. Loram, and T. M. M. Vieira, "Myoelectric activity along human gastrocnemius medialis: Different spatial distributions of postural and electrically elicited surface potentials," *J. Electromyogr. Kinesiol.*, vol. 23, no. 1, pp. 43–50, 2013.

[3] C. A. Angeli, V. R. Edgerton, Y. P. Gerasimenko, and S. J. Harkema, "Altering spinal cord excitability enables voluntary movements after chronic complete paralysis in humans," *Brain*, vol. 137, no. 5, pp. 1394–1409, 2014.

[4] J. A. Taylor, G. Picard, and J. J. Widrick, "Aerobic Capacity With Hybrid FES Rowing in Spinal Cord Injury: Comparison With Arms-Only Exercise and Preliminary Findings With Regular Training," *PM R*, vol. 3, no. 9, pp. 817–824, 2011.

[5] J. M. Shefner, "Motor unit number estimation in human neurological diseases and animal models," *Clin. Neurophysiol.*, vol. 112, no. 6, pp. 955–964, 2001.

[6] M. Popovic and T. Keller, "Modular transcutaneous functional electrical stimulation system," *Med. Eng. Phys.*, vol. 27, no. 1, pp. 81–92, 2005.

[7] H. C. Wu, S. T. Young, and T. S. Kuo, "A versatile multichannel direct-synthesized electrical stimulator for FES applications," *IEEE Trans. Instrum. Meas.*, vol. 51, no. 1, 2002.

[8] J. C. Jarvis and S. Salmons, "The application and technology of implantable neuromuscular stimulators: An introduction and overview," *Med. Eng. Phys.*, vol. 23, no. 1, 2001.

[9] J. Wang, H. Wang, T. He, B. He, N. V. Thakor, and C. Lee, "Investigation of Low-Current Direct Stimulation for Rehabilitation Treatment Related to Muscle Function Loss Using Self-Powered TENG System," *Adv. Sci.*, vol. 6, no. 14, 2019.

[10] J. Wang, H. Wang, N. V. Thakor, and C. Lee, "Self-Powered Direct Muscle Stimulation Using a Triboelectric Nanogenerator (TENG) Integrated with a Flexible Multiple-Channel Intramuscular Electrode," *ACS Nano*, vol. 13, no. 3, 2019.

[11] A. J. McComas, P. R. Fawcett, M. J. Campbell, and R. E. Sica, "Electrophysiological estimation of the number of motor units within a human muscle.," *J. Neurol. Neurosurg. Psychiatry*, vol. 34, no. 2, pp. 121–131, Apr. 1971.

[12] D. M. Hettinga and B. J. Andrews, "Oxygen consumption during functional electrical

This article has been accepted for publication in a future issue of this journal, but has not been fully edited. Content may change prior to final publication. Citation information: DOI 10.1109/ACCESS.2021.3133096, IEEE Access

IEEE Access

Cerone et al: Design of a programmable and modular neuromuscular electrical stimulator integrated into a wireless Body Sensor Network

stimulation-assisted exercise in persons with spinal cord injury: Implications for fitness and health," *Sport. Med.*, vol. 38, no. 10, pp. 825–838, 2008.

[13] P. H. Peckham and J. S. Knutson, "Functional electrical stimulation for neuromuscular applications.," *Annu. Rev. Biomed. Eng.*, vol. 7, pp. 327–60, 2005.

[14] M. Kjaer, "Why exercise in paraplegia?," *Br. J. Sports Med.*, vol. 34, no. 5, pp. 322–323, 2000.

[15] R. Davoodi and B. J. Andrews, "Switching curve control of functional electrical stimulation assisted rowing exercise in paraplegia.," *Med. Biol. Eng. Comput.*, vol. 41, no. 2, pp. 183–189, Mar. 2003.

[16] R. Davoodi, B. J. Andrews, and G. D. Wheeler, "Automatic finite state control of FES-assisted indoor rowing exercise after spinal cord injury," *Neuromodulation*, vol. 5, no. 4, pp. 248–255, 2002.

[17] S. C. Huerta, M. Tarulli, A. Prodic, M. R. Popovic, and P. W. Lehn, "A universal functional electrical stimulator based on merged flyback-SC circuit," in *15th International Power Electronics and Motion Control Conference and Exposition, EPE-PEMC 2012 ECCE Europe*, 2012.

[18] G. L. Cerone, T. M. M. Vieira, A. Botter, and M. Gazzoni, "Design of a Wireless, Modular and Programmable Neuromuscular Electrical Stimulator*," in *Proceedings of the Annual International Conference of the IEEE Engineering in Medicine and Biology Society, EMBS*, 2019.

[19] F. Del Pozo and J. M. R. Delgado, "Hybrid Stimulator for Chronic Experiments," *IEEE Trans. Biomed. Eng.*, vol. 25, no. 1, pp. 92–94, 1978.

[20] M. Valtin, K. Kociemba, C. Behling, B. Kuberski, S. Becker, and T. Schauer, "A versatile mobile stimulation system for transcutaneous FES RehaMovePro: A versatile mobile stimulation system for transcutaneous FES applications," *Eur J Transl Myol*, vol. 26, no. 3, pp. 203–208, 2016.

[21] J. Arnin, T. Yamsa-ard, P. Triponyuwasin, and Y. Wongsawat, "Development of practical functional electrical stimulation cycling systems based on an electromyography study of the Cybathlon 2016," *Eur. J. Transl. Myol.*, vol. 27, no. 4, pp. 295–301, 2017.

[22] J. J. Laskin *et al.*, "Electrical stimulation-assisted rowing exercise in spinal cord injured people. A pilot study.," *Paraplegia*, vol. 31, no. 8, pp. 534–541, 1993.

[23] B. Andrews, R. Gibbons, and G. Wheeler, "Development of Functional Electrical Stimulation Rowing: The Rowstim Series," *Artif. Organs*, vol. 41, no. 11, pp. E203--E212, Nov. 2017.

[24] IEC, "IEC 60601-1:2005 - Medical electrical equipment Part 1: General requirements for basic safety and essential performance." p. 426, 2005.

[25] J. Rosell, J. Colominas, P. Riu, R. Pallas-Areny, and J. G. Webster, "Skin Impedance From 1 Hz to 1 MHz," *IEEE Trans. Biomed. Eng.*, 1988.

[26] M. Knaflitz and R. Merletti, "Suppression of Simulation Artifacts from Myoelectric-Evoked Potential Recordings," *IEEE Trans. Biomed. Eng.*, vol. 35, no. 9, pp. 758–763, 1988.

[27] R. E. Fary and N. K. Briffa, "Monophasic electrical stimulation produces high rates of adverse skin reactions in healthy subjects," *Physiother. Theory Pract.*, vol. 27, no. 3, pp. 246–251, 2011.

[28] I. Moll *et al.*, "Functional electrical stimulation of the ankle dorsiflexors during walking in spastic cerebral palsy: a systematic review," *Developmental Medicine and Child Neurology*, vol. 59, no. 12. 2017.

[29] G. L. Cerone, A. Botter, and M. Gazzoni, "A Modular, Smart, and Wearable System for High Density sEMG Detection," *IEEE Trans. Biomed. Eng.*, vol. 66, no. 12, pp. 3371–3380, 2019.

[30] G. L. Cerone and M. Gazzoni, "A wireless, minaturized multi-channel sEMG acquisition system for use in dynamic tasks," in *2017 IEEE Biomedical Circuits and Systems Conference, BioCAS 2017 - Proceedings*, 2018.

[31] J. L. Vargas Luna, M. Krenn, J. A. Cortés Ramírez, and W. Mayr, "Dynamic impedance model of the skin-electrode interface for transcutaneous electrical stimulation," *PLoS One*, vol. 10, no. 5, 2015.

[32] A. Botter, G. Oprandi, F. Lanfranco, S. Allasia, N. A. Maffiuletti, and M. A. Minetto, "Atlas of the muscle motor points for the lower limb: Implications for electrical stimulation procedures and electrode positioning," *Eur. J. Appl. Physiol.*, vol. 111, no. 10, 2011.

[33] T. Vieira, P. Potenza, L. Gastaldi, and A. Botter, "Electrode position markedly affects knee torque in tetanic, stimulated contractions," *Eur. J. Appl. Physiol.*, vol. 116, no. 2, pp. 335–342, 2016.

[34] A. Botter, F. Lanfranco, R. Merletti, and M. A. Minetto, "Myoelectric fatigue profiles of three knee extensor muscles," *Int. J. Sports Med.*, vol. 30, no. 6, pp. 408–417, 2009.

[35] G. L. Cerone, A. Giangrande, M. Ghislieri, M. Gazzoni, H. Piitulainen, and A. Botter, "Design and validation of a wireless Body Sensor Network for integrated EEG and HD-sEMG acquisitions," *Under Revis.*

[36] A. Delorme *et al.*, "EEGLAB, SIFT, NFT, BCILAB, and ERICA: New tools for advanced EEG processing," *Comput. Intell. Neurosci.*, vol. 2011, 2011.

[37] A. Ojeda, N. Bigdely-Shamlo, and S. Makeig, "MoBILAB: An open source toolbox for analysis

and visualization of mobile brain/body imaging data," *Front. Hum. Neurosci.*, vol. 8, no. MAR, 2014.